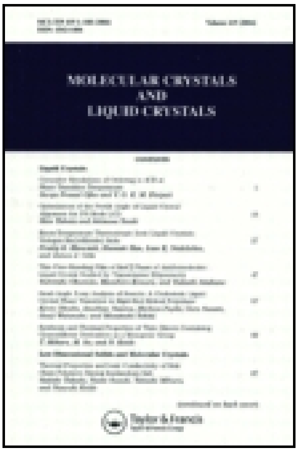

Molecular Crystals and Liquid Crystals
Publication details, including instructions for authors and subscription information:
http://www.tandfonline.com/loi/gmcl20

Electron Transport in Polymeric μ-Cyclopentadienylelement Complexes of the Main Group Elements

Yukihito Matsuura [a]

[a] Department of Chemical Engineering, Nara National College of Technology, Yamato-koriyama, Nara, Japan

To cite this article: Yukihito Matsuura (2012): Electron Transport in Polymeric μ-Cyclopentadienylelement Complexes of the Main Group Elements, Molecular Crystals and Liquid Crystals, 569:1, 103-111

To link to this article: http://dx.doi.org/10.1080/15421406.2012.689575

Mol. Cryst. Liq. Cryst., Vol. 569: pp. 103–111, 2012
Copyright © Taylor & Francis Group, LLC
ISSN: 1542-1406 print/1563-5287 online
DOI: 10.1080/15421406.2012.689575

Electron Transport in Polymeric μ-Cyclopentadienylelement Complexes of the Main Group Elements

YUKIHITO MATSUURA*

Department of Chemical Engineering, Nara National College of Technology,
Yamato-koriyama, Nara, Japan

I examined electrical conduction in polymeric μ-cyclopentadienylelement (Cp-E) complexes of the main group elements using the nonequilibrium Green's function formalism with the density functional theory. The polymeric Cp-E complexes of group 1 elements, which had ionic Cp-E bonds, showed very low conductance. In contrast, the polymeric Cp-E complexes of groups 13 and 14 elements exhibited enhanced n-type electrical conduction when a bias was applied between the electrodes, because the delocalized electronic states of the lowest unoccupied molecular orbital were within the bias window.

Keywords: Cyclopentadienyl complex; DFT; electron transport; NEGF

Introduction

Ferrocene, a cyclopentadienyl (Cp)-Fe sandwich complex, has stable oxidation-reduction characteristics and can be used for fabricating nano- and molecular electronic devices [1]. Other Cp transition metal complexes have been utilized as catalysts in the synthesis of organic compounds and polymers [2]. Polymeric μ-cyclopentadienylelement (Cp-E) complexes, shown in Figs 1(a), (b), and (c), are considered promising candidate materials for nano- and molecular electronic devices because the chemical structures of the complexes can be modified to obtain the desired electrical, optical, and magnetic properties. For example, gas-phase oligomeric Cp complexes of transition metals were predicted to have ferromagnetic properties [3]. In polymeric Cp-E complexes of the main group (group 1, 13, and 14) elements, the characteristics of the Cp-E bond varied from highly ionic to predominantly covalent, depending on the electronegativity of the elements, which differs from that of transition metals [4]. The variety of properties and bonding characteristics of the main group elements contributed to some of the distinct structural trends in the polymeric or oligomeric compounds. Some of the group 1 elements, Li and Na, formed polymeric Cp-E complexes with parallel sandwich geometry (Fig. 1(a)) [5]; on the other hand, other group 1 elements such as K and Cs, and group 13 elements In and Tl formed complexes with nonparallel inverse-sandwich structures, such as zigzag structures (Fig. 1(b)) [5–8]. The tricoordinate Cp-Pb complex adopts a branched polymeric structure; each Pb center is composed of two μ-Cp ligands and one terminal Cp ligand (Fig. 1(c)) [9,10]. The

---

*Address correspondence to Yukihito Matsuura, Department of Chemical Engineering, Nara National College of Technology, 22 Yatacho, Yamato-koriyama, Nara 639-1080, Japan. E-mail: matsuura@chem.nara-k.ac.jp

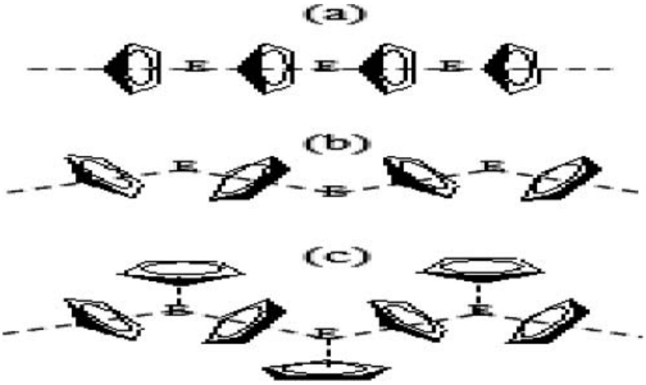

Figure 1. Configuration of Cp-E complex of (a) the parallel sandwich Cp arrangement, (b) nonparallel inverse sandwich arrangement, and (c) branched polymellic structure.

variety of chemical structures and electronic states of the complexes of elements belonging to different groups may afford unique electrical, magnetic, and optical properties to the complexes, making them suitable for use in molecular sensors, molecular switches, and molecular circuits.

Recently, electrical conduction at the nanometer scale was studied using nonequilibrium Green's function (NEGF) formalism with the density functional theory (DFT) [11]. NEGF calculations revealed that the above mentioned Cp-E complexes of transition metals exhibit ferromagnetic characteristics and spin-filtering behavior [12]. Similar to Cp-transition-metal complexes, Cp-E complexes of the main group elements may have unique electronic properties because they also show partial covalent bonding character, and this would result in some differences between the electrical and magnetic properties of the transition metal and main group element complexes. In this study, I calculated the electron transport in the main-group-element Cp-E complexes between two gold electrodes and analyzed the dependence of the Cp-E bond characteristics on the electrical conduction. In particular, I compared the electrical conduction of the Cp-E complexes of the sixth-period main group elements, which had zigzag structures, as described in Figs 1(b) and (c). Though Cs and Tl ions tend to be monovalent cations and the Pb ion tends to be a divalent cation, I selected the complexes in order to examine the variation in the electrical conduction with the typical element of the same period.

Calculation

I constructed an oligomer model of the Cp-E complexes sandwiched between two Au electrodes, as shown in Figs 2(a) and (b). The effect of metal–metal interaction on the electrical conduction of molecules with a minimum molecular size was examined by using models with two metal atoms in the complex. Since all the Cp rings have six π-electrons in their complexes, in our models, these complexes were treated as the anions $[Cp_3Cs_2]^-$, $[Cp_3Tl_2]^-$, and $[Cp_3Pb_2]^-$. To examine the electrical conduction of the complex growing on the gold electrode as a crystal, I used the data about bond lengths, bond angles, and torsion angles of the complexes of the crystal provided in the literature [4,6,8,9]. A research group has previously ascertained that the results of X-ray structure analysis of

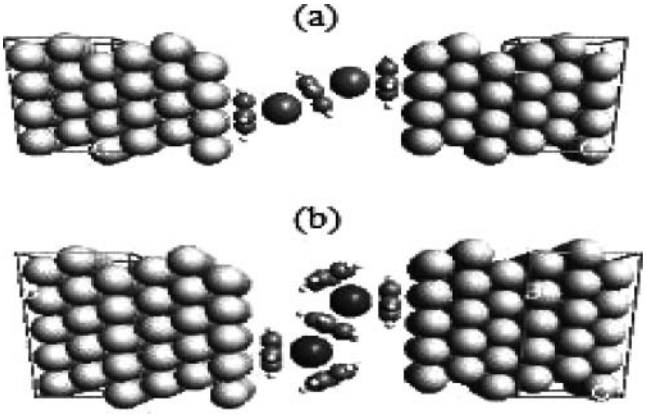

Figure 2. Device configuration of (a) Cp-E complex (E = Cs and Tl) and (b) Cp-Pb complex between the gold electrodes.

$[Cp_3Cs_2]^-$ and $[Cp_3Tl_2]^-$ coincide well with the optimized geometry under the DFT [13]. In this study, because of our computational capability, I could calculate the electrical conduction in one complex sandwiched between the two gold electrodes. The structural parameters are shown in Table 1. The Cp rings at the end of the complexes were aligned parallel to the Au(111) surface because this alignment was energetically stable [14]. The shortest C–Au distance was determined to be 2.90 Å, as was the case in our previous study [15–17]. The length of the Au–Au bond in the face-centered cubic Au crystal was the default value (2.88 Å) in program package, as mentioned below.

To examine the electrical conduction in the Cp-E complexes between the electrodes, I constructed a scattering region that included the complexes and three Au layers with a lateral (4 × 5) supercell as part of the electrodes. The Cp rings at the end of the complexes were attached to the Au(111) surfaces positioned to the right and left of the three Au layers in the scattering region. Electron transport calculations were carried out using a program based on the NEGF formalism with the DFT. I used the Atomistix Toolkit, which is based on the SIESTA code [18,19]. For the DFT calculation, I employed a single-ζ basis set with a single set of polarization functions and used the pseudopotential method with local density approximation for exchange correlation. The mesh cut-off energy was set at 75 Ry in the calculation.

Table 1. $Cp_{centroid}$-E distances and $Cp_{centroid}$-E-$Cp_{centroid}$ angles, conductances, and atomic charges of element E of Cp-E complexes (E = Cs, Tl, and Pb)

E	d (Å)	θ (°)	Conductance (μS)	Charge of E
Cs	2.82	138	6.83×10^{-3}	+0.809
Tl	3.19	137	3.17×10^{-2}	+0.491
Pb	2.72 (2.89)	120	6.74×10^{-1}	+0.880

d is $Cp_{centroid}$-E distance. d in parenthesis is the distance of terminal Cp ring.
θ is $Cp_{centroid}$-E-$Cp_{centroid}$ angle.

The transmittance ($T(E)$) at energy E was calculated from the following formula:

$$T(E) = Tr[\Gamma_L G \Gamma_R G^+], \tag{1}$$

where Γ_i ($i = L, R$) and G/G^+ are the coupling strength introduced by the self-energies of the left/right electrodes ($i = L, R$) and the retarded/advanced Green's function of the scattering region, respectively. The conductance was calculated from $T(E)$ at the Fermi energy level (E_F) as described below:

$$\text{Conductance} = \frac{2e^2}{h} T(E_F). \tag{2}$$

Finally, I could obtain the current $I(V)$ under bias V from the following equation:

$$I(V) = \frac{2e}{h} \int_{E_F - \frac{1}{2}eV}^{E_F + \frac{1}{2}eV} T(E)\, dE. \tag{3}$$

Results and Discussion

The I-V curves of Cp-E complexes are shown in Fig. 3. When the voltage between the electrodes was increased, the conduction in the Cp-Pb and Cp-Tl complexes also increased. Table 1 lists the high electrical conductance values of the Cp-Pb and Cp-Tl complexes. These complexes were considered to have covalent Cp-E bonds. In contrast, the conductance of the Cp-Cs complex was relatively low, suggesting that the Cp-Cs bond was ionic. To explain the difference between the electrical conduction in the Cp-E complexes, I analyzed the transmission spectra and molecular projected self-consistent Hamiltonian states of the complexes.

Subsequently, I calculated the electrical conduction in the case of the Cp-Cs complex. The near-zero transmission at the Fermi level resulted in very low conductance in the complex. The atomic charges shown in Table 1 indicated that one electron migrates from the Cs atom to the Cp rings, thus implying the ionic character of the Cp-E bond. As shown in Fig. 4, the highest occupied molecular orbital (HOMO) of the Cp-Cs complex indicated that the incident wave from the left electrode could not reach the right electrode to localize the electrons at the left end of the complex. The lowest unoccupied molecular orbital (LUMO)

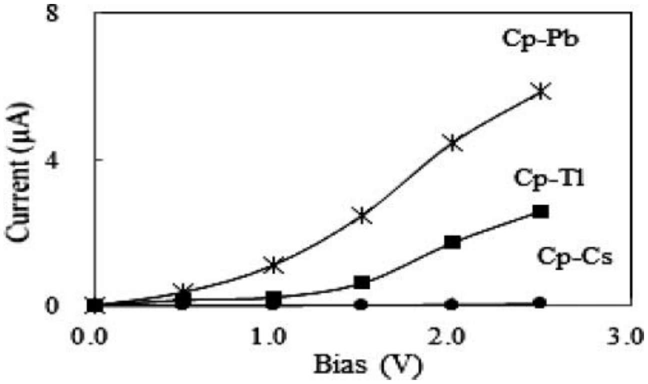

Figure 3. I-V curves of Cp-E complex (E = Cs, Tl, and Pb) between the gold electrodes.

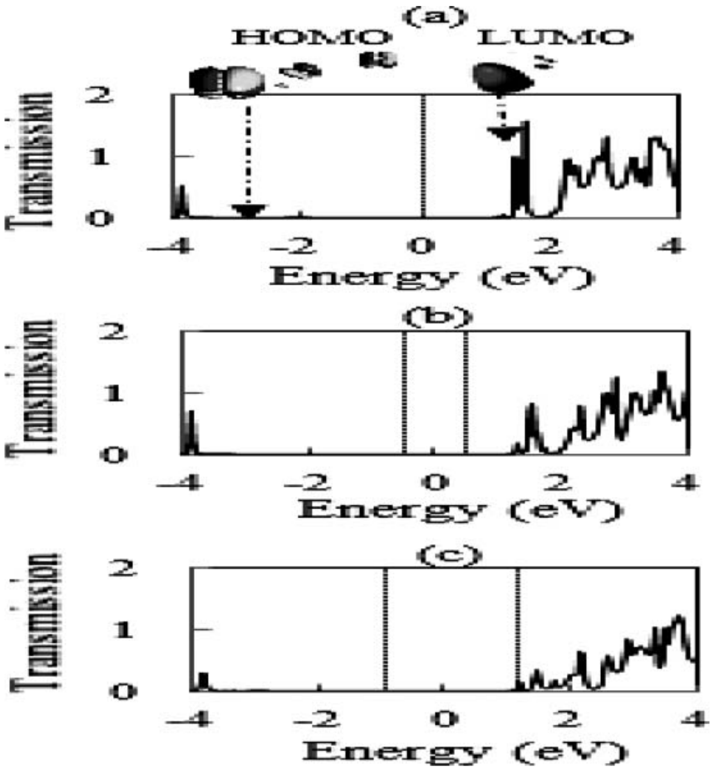

Figure 4. Transmission spectra of Cp-Cs complex between the gold electrodes under bias = (a) 0 V, (b) 1.0 V, and (c) 2.0 V.

of the Cp-Cs complex was located closer to the Fermi level than was the HOMO. Therefore, when the bias was applied to the scattering region between the electrodes, n-type electrical conduction through the LUMO occurred. As shown in Fig. 4(c), the LUMO level was not in the bias window even at a voltage of 2.0 V, and consequently, the Cp-Cs complex showed very low conduction even at high voltages.

I also calculated the electrical conduction of the Cp-Tl complex. As shown in Fig. 5 and Table 1, the current and the conductance of the Cp-Tl complex are relatively higher than those in the case of the Cp-Cs complex. Though the Cp–Tl distance is greater than the Cp–Cs distance, the Cp-Tl complex exhibits higher conductance. This is because of the covalent bond character, whereas the atomic charge values in Table 1 suggest a certain degree of localization of electrons in the Cp ring due to the electronegativity of the carbon atom. The HOMO primarily consisted of the Cp π-orbitals of the complex. In contrast, the LUMO consisted of the Tl 5p orbitals and the Cp π-orbitals. Since the LUMO was close to the Fermi level, the electrical conduction was influenced by the LUMO when a bias was applied between the gold electrodes. When a voltage of 2.0 V was applied to the complex, the right edge of the bias window overlapped with the left edge of the transmission peak/curve through the LUMO at -1.7 eV. A slight increase in the current at high voltages led to n-type conduction.

Finally, I investigated the electrical conduction of the Cp-Pb complex (group 14 elements). Although this complex has a paddle-wheel-like structure in which the Pb atom bears a third terminal Cp ring, as shown in Fig. 1(b), the electrical conduction is similar to

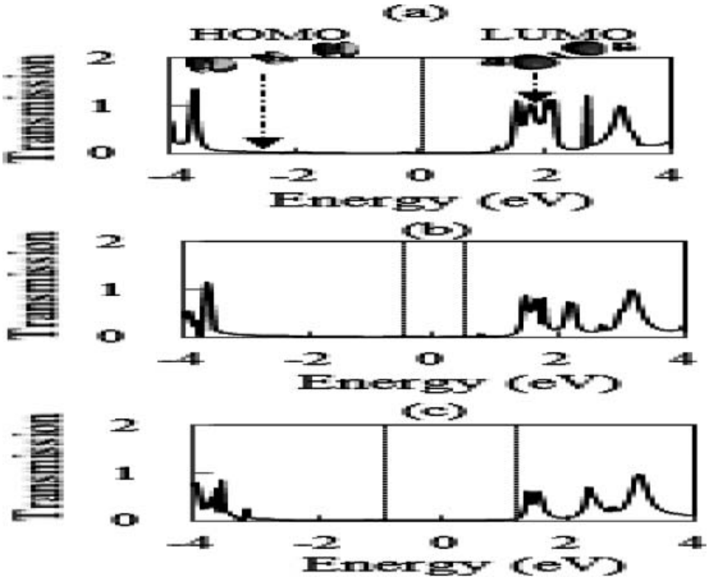

Figure 5. Transmission spectra of Cp-Tl complex between the gold electrodes under bias = (a) 0 V, (b) 1.0 V, and (c) 2.0 V.

that in the case of group 13 elements. As shown in Table 1, the conductance of the Cp-Pb complex is very high in comparison with that of other complexes. The relatively short Cp–Pb distance also influences the high electrical conduction. To analyze the electrical conduction, I examined the transmission by varying the bias between the gold electrodes. The atomic charge of Pb was close to +1, because the presence of one terminal Cp ring resulted in a tricoordinate environment around the Pb atom. A certain degree of localization of the electrons in the Cp ring was also caused by the difference in the electronegativity between Pb and C. As shown in Fig. 6(a), the HOMO formed by the Cp π-orbitals is located at an energy level of −2.1 eV and may not contribute much to the electron transport. In contrast, the energy level of the LUMO formed primarily by the Pb 5p orbitals was close to the Fermi level. When a high voltage of 2.0 eV was applied to the scattering region, the transmission caused by the LUMO (Fig. 6(c)) was within the bias window, which increased the conduction. This implies that tunneling through the Pb 5p orbitals is the main channel for electrical conduction.

In general, for Pb, Tl, and Au, the relativistic effect plays an important role in the electronic structure [20]. Although, the Atomistix Toolkit program cannot perform the calculation by including the effect, the electrical conduction of systems of an organic compound sandwiched between the two gold electrodes has been discussed qualitatively at this point [12,18,19]. Since, in this study, I have not considered the relativistic effect for Pb, Tl, and Au, I note that the discussion was qualitative and that in future, we will attempt to take the effect into consideration in the calculations. However, we can qualitatively discuss the characteristics of electrical conduction in the Cp-E complex. In my previous study, an energy band with a high density of states (DOS) was formed by Au 5d orbitals at the deep energy level, whereas Au 6s orbitals with a low DOS spread over a wide range of energy levels around the Fermi level [15]. In general, it is known that the relativistic effects lead to a reduction in the energy levels of the Au 6s/6p orbitals [20]. Therefore, in the

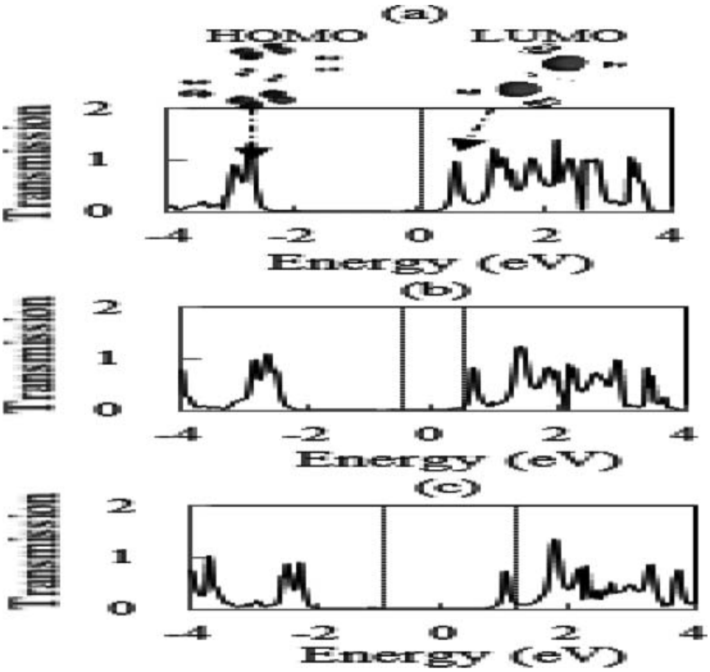

Figure 6. Transmission spectra of Cp-Pb complex between the gold electrodes under bias = (a) 0 V, (b) 1.0 V, and (c) 2.0 V.

system of the Cp-E complex sandwiched between the gold electrodes, a decrease in the DOS of the Au 6s orbitals at the energy level around the Fermi level reduces the interaction between the Cp-E complex and the gold electrode, resulting in sharp and small transmission peaks. As a result, the relativistic effects would reduce the electrical conduction in the Cp-E complex.

In this study, as mentioned above, the Cp-E complexes are determined to be anions because all Cp rings have six π-electrons. In general, an excess charge should induce the image force to reduce the barrier height and increase the tunneling probability [21–23]. To verify the image potential induced by the electronic polarization of the Cp-E complex, further calculations were carried out by including a counter cation in the system of the Cp-E complex. However, it is difficult to construct an oligomer model having a counter cation because these complexes have a polymeric structure. In this calculation, with reference to the structure of tris(cyclopentadienyl)lead(II) complex [22], the sodium cation was selected as a countercation of the Cp-Pb complex, in which Pb and Na were located at the opposite face of the equatorial Cp plane with a distance of 2.325 Å between the Cp ring and the Na atom, as shown in Fig. 7(a). Fast Fourier transform-based Poisson solver was used as a boundary condition of a direction parallel to the surface of electrodes to introduce a periodicity of a Cp-Pb-Na complex [18]. Furthermore, to verify the influence of the image force on the electrical conduction in the Cp-E complexes, instead of artificially introducing image charges in the system, the unit cell size of the gold electrodes was altered to be three Au layers with a lateral (5 × 5) supercell. As shown in Fig. 7(b), the transmission peaks at the deep energy levels around −2 eV changed, whereas the transmission peaks at the energy levels near the Fermi level were very small, similar to those shown in Fig. 6(a),

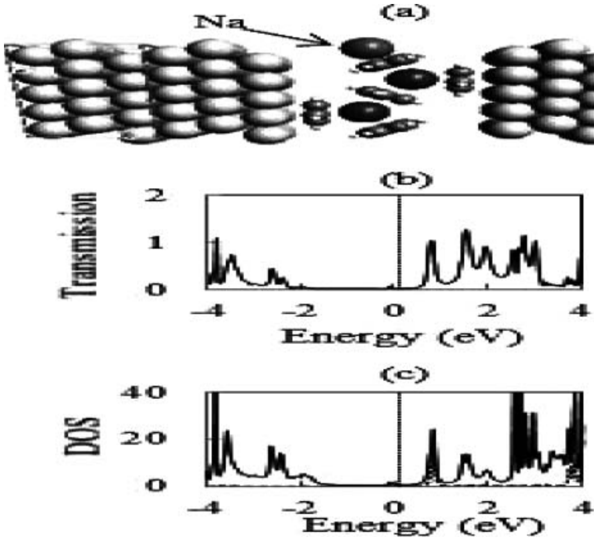

Figure 7. (a) Configuration, (b) transmission spectrum, (c) TDOS (solid line) and PDOS for Na atom (dotted line) of Cp-Pb-Na complex between the gold electrodes.

resulting in almost no change in the electrical conduction in the Cp-Pb complex. Fig. 7(c) indicates that the transmission peak at 0.78 eV is affected by the projected density of states (PDOS) for the Na 3s orbital, which does not directly influence the electrical conduction. Therefore, the existence of the counter cation and the variation in the unit cell size of the electrodes influenced the electrical conduction in the Cp-Pb complex slightly.

Conclusion

I have examined electrical conduction in the Cp-E complexes of the sixth-period main group elements using the NEGF formalism with the DFT. The Cp-E complexes tended to exhibit n-type electrical conduction. The Cp-Cs complex showed low electrical conduction because of the limited transmission in the bias window even at high voltages. On the other hand, the Cp-Tl and Cp-Pb complexes showed n-type electrical conduction because of the delocalized LUMO states. The electrical conduction of the complexes is because of the energy level of LUMO formed by the d orbitals of the metal atom.

References

[1] Manners, I. (2002). *Synthetic Metal Containing Polymers*, Wiley-VCH: New York.

[2] Xu, Z., Xie, Y., Feng, W., & Schaefer, H. F. III. (2003). *J. Phys. Chem. A*, *107*, 2716.

[3] Nagao, S., Kato, A., Nakajima, A., & Kaya, K. (2000). *J. Am. Chem. Soc.*, *122*, 4221.

[4] Jutzi, P., & Burford, N. (1999). *Chem. Rev.*, *99*, 969.

[5] Dinnebier, R. E., Behrens, U., & Olbrich, F. (1997). *Organometallics*, *16*, 3855.

[6] Harder, S., & Prosenc, M. H. (1996). *Angew. Chem., Int. Ed. Engl.*, *35*, 97.

[7] Beachley, O. T. Jr., Pazil, J. C., Glassman, T. E., Churchill, M. R., Fettinnger, J. C., & Blom, R. (1988). *Organometallics*, *7*, 1051.

[8] Berar, J. F., Calvarin, G., Pommier, C., & Weigel, D. (1975). *J. Appl. Crystallogr.*, *8*, 386.

[9] Panattoni, C., Bombieri, G., & Croatto, U. (1966). *Acta Crystallogr.*, *21*, 823.

[10] Overby, J. S., Hanusa, T. P., & Young, V. G. Jr. (1998). *Inorg. Chem.*, *37*, 163.
[11] Datta, S. (2005). *Quantum Transport: Atom to Transistor*, Cambridge: Cambridge University Press.
[12] Yi, Z., Shen, X., Sun, L., Shen, Z., Hou, S., & Sanvito, S. (2010). *ACS Nano*, *4*, 2274.
[13] Sansores, L. E., Salcedo, R., & Flores, H. (1999). *J. Mol. Struct. (THEOCHEM)*, *460*, 37.
[14] Brizuela, G., & Hoffmann, R. (1998). *J. Phys. Chem.*, *102*, 9618.
[15] Matsuura, Y., & Uchimya, R. (2010). *Solid State Commun.*, *150*, 1400.
[16] Matsuura, Y. (2011). *Solid State Commun.*, *151*, 1877.
[17] Matsuura, Y. (2012). *Appl. Phys. Lett.*, *100*, 53303.
[18] Atomistix Toolkit, Quantumwise A/S, available at: www.quantumwise.com. Accessed April 1, 2011.
[19] Stokbro, K. (2008). *J. Phys.: Condens. Matter.*, *20*, 64216.
[20] Reiher, M., & Wolf, A. (2009). *Relativistic Quantum Chemistry*, Berling, Germany: Wiley-VCH.
[21] Ma, X. C., Shu, Q. Q., Meng, S., & Ma, W. G. (2003). *Thin Solid Films*, *436*, 292.
[22] Simmons, J. G. (1963). *J. Appl. Phys.*, *34*, 2581.
[23] Brinkman, W. F., Dynes, R. C., & Rowell, J. M. (1970). *J. Appl. Phys.*, *41*, 1915.